

Criticality and entanglement in random quantum systems

G. Refael

Department of Physics, California Institute of Technology, MC 114-36, 1200 E. California Blvd., Pasadena, CA 91125

J. E. Moore

Department of Physics, University of California, Berkeley, CA 94720
Materials Sciences Division, Lawrence Berkeley National Laboratory, Berkeley, CA 94720

Abstract. We review studies of entanglement entropy in systems with quenched randomness, concentrating on universal behavior at strongly random quantum critical points. The disorder-averaged entanglement entropy provides insight into the quantum criticality of these systems and an understanding of their relationship to non-random (“pure”) quantum criticality. The entanglement near many such critical points in one dimension shows a logarithmic divergence in subsystem size, similar to that in the pure case but with a different universal coefficient. Such universal coefficients are examples of universal critical amplitudes in a random system. Possible measurements are reviewed along with the one-particle entanglement scaling at certain Anderson localization transitions. We also comment briefly on higher dimensions and challenges for the future.

1. Introduction

Several important connections have been established in recent years between concepts from quantum information and problems in many-body physics. One such connection is the use of entanglement entropy to understand how ground states of various quantum Hamiltonians show either criticality or topological order. This article reviews recent work on entanglement entropy in systems with quenched randomness, and will focus for the most part on universal behavior connected with strongly random quantum critical points. Beyond improving the general understanding of entanglement in many-particle systems, these studies have given useful insight into random quantum critical points. For example, entanglement entropy provided the first example of a universal “critical amplitude” at this type of critical point.

In this introduction, we review the basic concept of entanglement entropy and a few of its applications to non-random systems, then introduce the physics of strongly random quantum critical points. These critical points are best understood in one spatial dimension, where the real-space renormalization group (RSRG) approach gives nonperturbative results for many disordered-averaged quantities that are believed to be exact. In some cases, such as the random XX spin chain that is connected to free fermions with random hopping via the Jordan-Wigner transformation, numerical results can confirm the RSRG predictions. We then discuss the possibility of experimental measurements and make some introductory comments about strongly random systems in higher dimensions. The later sections of this review are as follows: Sections 2 and 3 introduce infinite-randomness fixed points and calculations of their entanglement, Section 4 discusses possible experimental observations, Section 5 reviews single-particle entanglement in Anderson-type localization problems, Section 6 discusses numerical results, and Section 7 briefly introduces higher-dimensional results and some open problems for the future.

1.1. Entanglement entropy

A fundamental concept of quantum information is the entanglement entropy of a pure quantum state, defined as the von Neumann entropy of the reduced density matrix created by a partition of the system into parts A and B :

$$S = -\text{Tr } \rho_A \log_2 \rho_A = -\text{Tr } \rho_B \log_2 \rho_B. \quad (1)$$

Here the base-2 logarithm means that the entropy is measured in bits. If the original state is not a product state (i.e., does not factorize into a pure state for subsystem A and one for B), then the entanglement entropy is nonzero. Since it is determined by the reduced density matrix for a subsystem, which characterizes all physical measurements on that subsystem, there is no way to distinguish through measurements only on A whether an entropy arose from partition of an entangled pure state of AB or from a mixed state of AB .

In most cases we will be interested in partitions of an infinite system into a finite contiguous part A and a remainder B . Entanglement of the ground state of a local Hamiltonian is different from that of a generic state in the Hilbert space: the locality means that ground states with an energy gap to excitations typically show entanglement that scales with the size of the AB boundary (the “area law” [1, 2, 3]). This leads to the notion of a length scale around the boundary beyond which entanglement must decay rapidly. As reviewed in the following section, quantum critical points can violate the area law because, just as correlations become long-ranged at a quantum critical point, entanglement can do so as well. The increase at entanglement at quantum critical points seems to be a general property of both random and translational-invariant systems, and is clearest in one dimension as explained below.

A question occasionally raised is to what extent entanglement entropy and other quantum information concepts are either “useful” or “measurable” in condensed matter systems. The first use of quantum information, as in the above examples is to understand something new about condensed matter systems that is not evident in correlation functions or other more conventional quantities. Another important use, which we will not discuss here, arises from the fact that the entanglement entropy of a state is related to the accuracy with which it can be approximated by the matrix product states that are convenient for numerical simulations. Two examples from one-dimensional translationally invariant systems are that states satisfying the “area law” are described exponentially well by matrix product states, while for critical states [4, 5] the matrix product state description converges at a slower rate determined by the critical point’s central charge. Finally, while determination of the entanglement entropy by direct measurement of the reduced density matrix [6] indeed seems impracticable on a many-particle system, the variance of flux measurements on a spin chain [7] can be used to obtain the entanglement entropy. This proposed measurement is closely connected to efforts to determine the source of unusual flux noise in SQUID systems.

Two ways to generalize the entanglement entropy are via the “Renyi entropy” of the reduced density matrix

$$S_\alpha = \frac{1}{1-\alpha} \log_2 \text{Tr} \rho_A^\alpha, \quad (2)$$

which reduces to the (von Neumann) entanglement entropy as $\alpha \rightarrow 1$, or the “entanglement spectrum” (the full eigenvalue distribution of the reduced density matrix). The entanglement spectrum has been analyzed for phases with topological order [8] or translation-invariant quantum criticality [9, 5], and is discussed briefly below for the random singlet phase. At least for the random singlet phase, the entanglement spectrum and Renyi entropy are likely to follow quite directly from the ordinary entanglement entropy, but for more complicated random critical points this is not expected to be the case.

1.2. Quantum criticality

The entanglement entropy of the ground state at a quantum critical point can, in some cases, be understood via the quantum-to-classical mapping. An important example is furnished by the quantum critical points in one dimension that become two-dimensional conformal field theories (CFTs), where the entanglement entropy in the quantum theory has a logarithmic divergence, whose coefficient is connected to the central charge of the CFT: [10, 11, 12, 13]

$$\lim_{N \rightarrow \infty} S \sim \frac{c}{3} \log_2 N, \quad (3)$$

where we consider A as a finite contiguous set of N spins (or other local Hilbert space) and B is the complement of A in the infinite chain. Away from criticality, the entanglement S is bounded above as $N \rightarrow \infty$ (the one-dimensional version of the “area law”. [1]) Surprisingly, the entanglement entropy, whose definition is closely tied to the lattice via the Hilbert space is actually a universal property of the critical field theory, and hence independent of lattice details. Most one-dimensional translation-invariant critical points fall into this class: the key is being able to rescale space and time to obtain rotational invariance and thence conformal invariance (for example, $z = 2$ quantum critical points do not fall into this class). At this time we lack a similarly complete understanding of translation-invariant critical points in higher dimensions; isolated solvable cases include free fermions [14, 15], higher dimensional conformal field theories [13], and one class of $z = 2$ quantum critical points. [16]

The connection between the central charge of CFT’s and their entanglement entropy implies that indeed for quantum critical points with classical analogs, the natural measure of universal critical entropy in the quantum system (the entanglement entropy) is determined by the standard measure of critical entropy in the classical system (the central charge). In addition, it translates important notions about the central charge to the realm of the universal quantum measure - the entanglement entropy. Zamolodchikov’s c -theorem [17] states that the central charge c decreases along unitary renormalization-group (RG) flows. Therefore we conclude that the entanglement entropy of CFT’s also decreases along RG flows. Stated this way, the strength of the c -theorem may apply to universal critical entropies in quantum systems that are not tractable by the quantum-to-classical mapping.

Understanding universal behavior near quantum critical points has been a major goal of condensed matter physics for at least thirty years. Quantum critical points describe continuous phase transitions at zero temperature, where quantum-mechanical phase coherence exists even for the long-wavelength fluctuations that control the transition. Some quantum critical points can be understood via mapping to standard classical critical points in one higher dimension, but many of the most experimentally relevant quantum critical points do not seem to fall into this category. Furthermore, even quantum critical points that can be studied using the quantum-to-classical mapping have important universal features such as frequency-temperature scaling that do not appear at finite-temperature critical points. [18]

1.3. Random systems and infinite randomness phases

The properties of quantum critical points are often modified dramatically by introducing randomness in their Hamiltonians. Furthermore, the lower the dimensionality of the system, the more dramatic the effect of disorder is. Several examples will be discussed in this review. Anderson localization is the most Historically celebrated example; Anderson has shown that a random chemical potential can completely localize an otherwise propagating band [19] (see Sec. 5).

Another class of disorder induced phases was found when considering the random spin-1/2 Heisenberg chain [20, 21, 22, 23, 24]. A conclusive solution of the ground state was found by D. S. Fisher, [23] who showed that any amount of disorder will drive a spin-1/2 Heisenberg chain (as well as an easy-plane xxz chain, and an xx chain) to the random-singlet phase. As we discuss below (Sec. 2.1), in this phase, pairs of strongly interacting spins form singlets, which may span arbitrarily large distances. The random singlet phase is essentially a localized phase, with the *typical* spin-spin correlations decaying as $C^{typ}(L) \sim e^{-c\sqrt{L}}$. The typical correlations can be defined as the exponent of $\ln\langle\hat{S}^z(0)\hat{S}^z(L)\rangle$ (where an overline denotes disorder average). But if instead we consider the *average* correlations, we find that the average $\langle\hat{S}^z(0)\hat{S}^z(L)\rangle$ is dominated by the rare event of the two sites 0 and L being bound to a singlet. The probability of this is essentially geometric, and falls off as $1/L^2$. Therefore, $\langle\hat{S}^z(0)\hat{S}^z(L)\rangle \sim 1/L^2$ as well. [23, 25, 26, 27] The random singlet phase also arises as a localization problem of Majorana, as well as Dirac Fermions, as demonstrated in Refs. [28].

The RS phase is but one example of an *infinite randomness fixed point*. These points possess unique scaling properties. Contrary to the standard energy-length scaling at pure critical points, where $E \sim 1/L^z$, the infinite randomness fixed points are also gapless, but with the energy of an excitation scaling as:

$$\ln 1/E \sim L^\psi, \quad (4)$$

Furthermore, the low energy behavior of infinite-randomness fixed points is described by random Hamiltonians with universal coupling distributions:

$$\rho(J) \sim \frac{1}{J^{1-\chi/\Gamma}}, \quad (5)$$

$\Gamma = \ln \Omega_0/\Omega$ is a parameter which keeps track of the energy scale at which we probe the chain Ω , relative to its largest bare coupling Ω_0 . χ and ψ are universal constants, which at the random singlet phase take the values $\psi = 1/2$, $\chi = 1$. Other infinite randomness fixed points maintain the form of the scaling, Eqs. (4, 5), but with $\psi = 1/(n+1)$ and $\chi = n$ for other integer n (these numbers describe the Damle-Huse hierarchy; other combinations of ψ and χ may be possible).

The infinite-randomness fixed points are, loosely speaking, the random analogs of pure CFT's, and therefore it is important to understand all that we can about their special universal properties, such as their entanglement entropy. Generically, such points can be reached as instabilities to disorder of well-known CFT's (e.g. in the XX,

Heisenberg, and transverse-field Ising model). Also, as we shall review, random gapless systems exhibit RG flow between different infinite randomness fixed points. The study of the entanglement entropy in these systems allows us to explore any correspondence they may have with the pure CFT c-theorem. Namely, does the entanglement entropy, or a related measure, also decrease along flow lines of systems with randomness? This question can be broken into two: (a) does the entanglement entropy decrease along flows between pure CFT's and infinite-randomness fixed points? (b) does the entanglement entropy decrease along flows between two different infinite randomness fixed points?

We note here that infinite randomness physics also has higher dimensional analogs, as explored in Ref. [22], and especially by several groups [29, 30, 31]. While we concentrate mostly on disordered systems in 1d, Sec. 7 will review relevant work in higher dimensions.

2. Field guide to infinite-randomness fixed points

One can not truly appreciate infinite-randomness criticality without working through an example for each of the universality classes mentioned above. As of now, all known infinite-randomness universality classes belong to the Damle-Huse series with $\psi = 1/(n + 1)$ and $\chi = n$ [32]. The simplest systems which give rise to the Damle-Huse series are antiferromagnetic spin chains with $S = n/2$. Below we first review the random-singlet phase ($n = 1$) in the spin-1/2 Heisenberg model, and then proceed to analyze how $n > 1$ infinite-randomness critical points arise in spin- $n/2$ chains, and in non-abelian anyonic models.

2.1. Random-singlet phases - the simplest infinite randomness fixed points

The original infinite-randomness fixed point is the random singlet phase. This phase describes the ground state of a spin-1/2 antiferromagnetic Heisenberg chain with essentially any disorder distribution ‡. Without disorder, the low-energy behavior of the spin-1/2 Heisenberg chain is described by a conformal field theory with central charge $c = 1$. Upon introduction of disorder, the low-energy behavior of the chain flows to a different critical phase: the random-singlet phase. [22, 21, 23]

Let us write the random Heisenberg chain Hamiltonian:

$$\mathcal{H} = \sum_{i=1}^L J_i \hat{\mathbf{S}}_i \cdot \hat{\mathbf{S}}_{i+1} \quad (6)$$

Roughly speaking, the strongest bond in the chain, say, J_i , localizes a singlet between sites i and $i + 1$. Quantum fluctuations, treated within second-order perturbation theory, induce a new term in the Hamiltonian which couples sites $i - 1$ and $i + 2$: [20, 33]

$$\mathcal{H}'_{i-1, i+2} = \frac{J_{i-1} J_{i+1}}{2J_i} \hat{\mathbf{S}}_{i-1} \cdot \hat{\mathbf{S}}_{i+2}. \quad (7)$$

‡ Excluding freak distributions such as $\rho(J) \sim (J \ln^\alpha J)^{-1}$ with $\alpha > 1$.

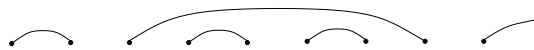


Figure 1. The ground state of the random Heisenberg model consists of singlets connecting spins over arbitrarily long length scales.(figure taken from Ref. [34])

Eq. (7) is the Ma-Dasgupta rule for the renormalization of strong bonds.

This simple observation opens the way for an iterative real-space renormalization group approach to random chains: we identify the strongest bond in the chain, put the two spins it connects into a singlet, and rewrite the Hamiltonian using the Ma-Dasgupta rule (7) without the two recently singletted spins, and with an effective and suppressed Heisenberg interaction between their neighbors. After carrying out this iteration many times, the active spins are a dilute irregular array compared to the initial chain. Therefore the singlets they form occur over large length scales, which increase as the decimation procedure progresses. The solution is complete when all spins have been paired into singlets, which automatically implies that the largest singlet connects spins separated by a length comparable with the size of the system. A sketch of this phase is given in Fig. 1.

A useful parametrization of the couplings in the analysis of the random spin-1/2 Heisenberg chain is:

$$\beta_i = \ln \frac{\Omega}{J_i} \quad (8)$$

where Ω is the highest energy in the Hamiltonian:

$$\Omega = \max_i \{J_i\}, \quad (9)$$

and plays the role of a UV cutoff. The advantage of this parametrization becomes clear when considering the Ma-Dasgupta rule in these variables:

$$J_{eff} = \frac{J_L J_R}{2\Omega} \rightarrow \beta_{eff} = \beta_L + \beta_R - \ln 2 \quad (10)$$

with L and R indicating bond to the left and to the right of the decimated bond. It is beneficial to define also a logarithmic RG flow parameter:

$$\Gamma = \ln \frac{\Omega_0}{\Omega} \quad (11)$$

where Ω_0 is an energy scale of the order of the maximum J_i in the bare Hamiltonian. In terms of these variables, and using the Ma-Dasgupta rule, Eq. (10), we can construct a flow equation for the distribution of couplings β_i :

$$\frac{dP(\beta)}{d\Gamma} = \frac{\partial P(\beta)}{\partial \beta} + P(0) \int_0^\infty d\beta_1 \int_0^\infty d\beta_2 \delta_{(\beta-\beta_1-\beta_2)} P(\beta_1) P(\beta_2). \quad (12)$$

Here the first term describes the reduction of Ω , and the second term is the application the Ma-Dasgupta rule, where we neglect $\ln 2$ in comparison to the β 's. For the sake of

readability, we denote the convolution with the cross sign:

$$P(\beta_1) \overset{\beta}{\times} R(\beta_2) = \int_0^\infty d\beta_1 \int_0^\infty d\beta_2 \delta_{(\beta-\beta_1-\beta_2)} P(\beta_1) R(\beta_2). \quad (13)$$

Eq. (12) has a simple solution, found by Fisher, which is an attractor to essentially all initial conditions and distributions: [23]

$$P(\beta) = \frac{\chi}{\Gamma} e^{-\chi\beta/\Gamma}. \quad (14)$$

with $\chi = 1$.

The function in Eq. (14) is the key to physical characteristics of the random-singlet phase. For instance, to obtain the energy-length scaling we make the following observations. Each decimation step removes two sites, and the probability for a site to be removed at RG scale $\Gamma \rightarrow \Gamma + d\Gamma$ is $P(\beta = 0)$. Therefore, the density of free spins evolves as:

$$\frac{dn}{d\Gamma} = -2nP(0) = -2\frac{n}{\Gamma} \quad (15)$$

which is solved by:

$$n = \frac{n_0}{\Gamma^2} \quad (16)$$

upto an offset of order 1 in Γ . The length of a singlet formed at RG scale Γ must be of order of the average distance between sites:

$$\ell \sim 1/n. \quad (17)$$

This can be put into the length-energy scaling:

$$\ell^\psi \sim \Gamma = \ln 1/E \quad (18)$$

with ψ being a universal critical exponent:

$$\psi = 1/2. \quad (19)$$

We note that almost exactly the same analysis applies to the easy-plane xxz chain: [23]

$$\mathcal{H} = J \sum_i \left(\hat{S}_i^x \cdot \hat{S}_{i+1}^x + \hat{S}_i^y \cdot \hat{S}_{i+1}^y + \lambda \hat{S}_i^z \cdot \hat{S}_{i+1}^z \right) \quad (20)$$

with $-1/2 < \lambda < 1$. Under real-space RG, the anisotropy parameter λ flows to zero, which implies that the xxz random-singlet phase is a fixed point distinct from its Heisenberg model analog at the isotropic $\lambda = 1$ point.

2.2. Transverse field Ising model

In addition to the Heisenberg model, early studies of infinite randomness phases concentrated on the transverse field Ising model (TFIM) [25]. The Hamiltonian of the random quantum Ising model is

$$\mathcal{H} = - \sum_i \left(J_{i,i+1} \hat{\sigma}_i^z \hat{\sigma}_{i+1}^z + h_i \hat{\sigma}_i^x \right) \quad (21)$$

with each site having two states, $\hat{\sigma}^z = \pm 1$, with quantum fluctuations between them caused by the transverse, $\hat{\sigma}^x$, fields. The system is illustrated in Fig. 2. The model has a global symmetry of inversion about the xy spin plane; breaking this symmetry with z fields would change the low energy physics radically.

The analysis of the random TFIM follows the analysis of the random Heisenberg model very closely, using real-space decimations of the strongest terms in the Hamiltonian. The Hamiltonian consists of two types of operators, $\hat{\sigma}_i^x$ and $\hat{\sigma}_i^z \hat{\sigma}_{i+1}^z$, both of which have eigenvalues ± 1 . Therefore it is natural to compare their coefficients, h_i and J_i directly. The iterative decimation step starts with finding the strongest coupling from the set $\{h_i, J_i\}_{i=1}^N$. If $h_i = \Omega$ is the largest coupling, the zeroth order solution of the wave function (i.e., ignoring all other couplings in the Hamiltonian) will be an eigenstate of $\hat{\sigma}_i^x$ obeying $\langle \hat{\sigma}_i^x \rangle = 1$. Second order perturbation analysis of the Ising bonds to the left and right of site i produces an Ising coupling:

$$\mathcal{H}_{i-1,i+1} = \frac{J_{i-1}J_i}{\Omega} \hat{\sigma}_{i-1}^z \hat{\sigma}_{i+1}^z. \quad (22)$$

The coefficient of this Ising coupling clearly obeys $J_{eff} < \Omega, J_i, J_{i-1}$. This is the TFIM analog of the Ma-Dasgupta decimation step. Similarly, if the strongest coupling is $J_i = \Omega$, the zeroth order solution of the wave function will be an eigenstate of $\hat{\sigma}_i^z \hat{\sigma}_{i+1}^z$ with $\langle \hat{\sigma}_i^z \hat{\sigma}_{i+1}^z \rangle = 1$. There are two states like that: $\hat{\sigma}_i^z = \hat{\sigma}_{i+1}^z = \pm 1$. The degeneracy is lifted through quantum fluctuations induced by the terms $-h_i \hat{\sigma}_i^x - h_{i+1} \hat{\sigma}_{i+1}^x$. Using second order perturbation theory we obtain:

$$\mathcal{H}_{i,i+1} = \frac{h_i h_{i+1}}{\Omega} \hat{\sigma}_i^x \hat{\sigma}_{i+1}^x = \frac{h_i h_{i+1}}{\Omega} \hat{\sigma}_{i,i+1}^x. \quad (23)$$

Eqs. (22, 23) are the TFIM analogs of the Ma-Dasgupta decimation step for the Heisenberg model.

The decimation steps of the TFIM are also simplified by using logarithmic variables for the Ising coupling and for the transverse field. We define:

$$\beta_i = \ln \frac{\Omega}{J_i} \quad \zeta_i = \ln \frac{\Omega}{h_i} \quad (24)$$

and also follow the definition for Γ , Eq. (11). The decimation steps then become additive. For a field decimation at site i , we have:

$$\beta_{eff} = \beta_i + \beta_{i+1}. \quad (25)$$

For a bond decimation, the effective field becomes

$$\zeta_{eff} = \zeta_i + \zeta_{i+1}. \quad (26)$$

The TFIM at low energies is characterized by coupling and transverse field distributions $P(\beta)$ and $R(\zeta)$ respectively, which obey the following flow equations:

$$\begin{aligned} \frac{dP(\beta)}{d\Gamma} &= \frac{\partial P(\beta)}{\partial \beta} + R(0)P(\beta_1) \overset{\beta}{\times} P(\beta_2) + P(\beta)(P(0) - R(0)), \\ \frac{dR(\zeta)}{d\Gamma} &= \frac{\partial R(\zeta)}{\partial \beta} + P(0)R(\zeta_1) \overset{\zeta}{\times} R(\zeta_2) + R(\zeta)(R(0) - P(0)). \end{aligned} \quad (27)$$

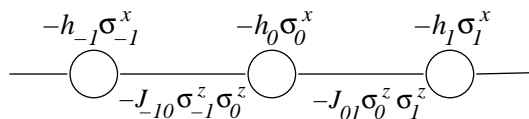


Figure 2. The Hamiltonian of the transverse field Ising model. Each site is a spin-1/2 that interacts via Ising exchange with its nearest neighbors and can be flipped by the local x -magnetic field. (Figure taken from Ref. [27])

The quantum Ising model exhibits a quantum phase transition in its ground state when the nearest neighbor interaction and the transverse field are of comparable strength. In a non-random model this occurs when $J = h$ [18]. In a random system, where the J 's and the h 's are drawn independently from some distributions, a solution of the flow equations (27) shows that the transition occurs when $\overline{\log h} = \overline{\log J}$, where the over-bars denote averaging over the randomness [25]. A convenient parametrization of the proximity to the transition is

$$\delta \equiv \frac{\overline{\log h_I} - \overline{\log J_I}}{\text{var}(\log h) + \text{var}(\log J)} \quad (28)$$

with $\delta > 0$ yielding the disordered phase, and $\delta < 0$ yielding the ferromagnetic phase, where a large cluster forms due to the Ising interaction. Using this parametrization, Fisher found that at low energies, at the fixed point, $\delta = 0$, and at the Griffiths phase that surrounds it, the distribution functions are given by:

$$P(\beta) = \frac{\delta e^{-\delta\Gamma}}{2 \sinh \delta\Gamma} e^{-(\delta + \delta \coth(\Gamma\delta))\beta} \quad R(\zeta) = \frac{\delta e^{\delta\Gamma}}{2 \sinh \delta\Gamma} e^{-(\delta + \delta \coth(\Gamma\delta))\zeta}. \quad (29)$$

As can be easily seen, when $\delta = 0$, the two distributions for coupling and transverse field become identical, and the low energy behavior of the random TFIM obeys the same infinite randomness scaling as the random singlet phase. The picture of the low energy phase, however, is quite different. During the renormalization process, as the energy scale is reduced, cluster of parallel spins form and grow to length scale ℓ , and then they freeze in a superposition of pointing up and down as clusters, i.e., in the x -direction of the collective spin. The excitation energy of such cluster scales as $e^{-\sqrt{\ell}}$. Entanglement entropy resides in the cluster formation: the entanglement entropy between two sections is equal to the number of clusters that connect them.

When δ is non-zero but small, the random TFIM is in a Griffiths phase, where the low energy behavior dominated by gapless but well localized excitations. Thinking about the low energy behavior using the decimation picture, at early stages the chain obeys the critical $\delta = 0$ scaling. But when the typical cluster sizes and bond lengths are of the same order of the *correlation length*

$$\xi \approx \frac{1}{\delta^2}, \quad (30)$$

and the log-energy scale is of order

$$\Gamma_{\times} \sim \frac{1}{\delta}, \quad (31)$$

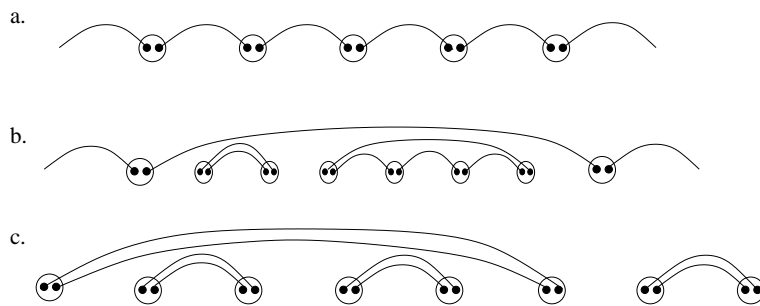


Figure 3. (a) At very low disorder, the ground state of the spin-1 Heisenberg chain is well described as a valence-bond solid. Each spin-1 site is described by two spin-1/2 parts (black dots) that are symmetrized. Each site forms a spin-1/2 singlet to its right and to its left. (b) As disorder grows, defects appear in the VBS structure, and the gap is suppressed. (c) At very high disorder, a phase transition occurs to the spin-1 random singlet (RS) phase.

a crossover to the ordered ($\delta < 0$) or disordered ($\delta > 0$) occurs. The energy-length scaling is then different from that at the critical point. For small δ , in both phases

$$\Omega \sim \ell^{-z(\delta)} \quad (32)$$

with the effective dynamical exponent,

$$z \approx \frac{1}{|\delta|} \quad (33)$$

near the critical point.

2.3. Infinite-randomness fixed points for higher spin

As mentioned in the beginning of this section, the random-singlet phase, with universal distribution (14) and length-energy scaling, Eq. (18) is but one example of an *infinite randomness fixed point*. In general, disordered systems may have a similar type of logarithmic length-energy scaling relations, Eq. (18), with different ψ and χ in Eq. (4, 5). As mentioned above, to date, all known universality classes of infinite-randomness fixed points can be realized in Heisenberg models with spin $s \geq 1/2$. Following Refs. [35, 36] and [34] which dealt with the spin-1 and spin-3/2 cases respectively, Damle and Huse showed that a spin- s chain may exhibit infinite-randomness fixed points with [32]:

$$1/\psi = 2s + 1, \quad \chi = 2s. \quad (34)$$

These fixed points were dubbed domain-wall symmetric fixed points.

2.3.1. Domain-wall picture The simplest illustration of the domain-walls picture is in the spin-1/2 random singlet phase. The random-singlet phase forms through a competition between two possible singlet domains: Domain (1,0) with singlets appearing on odd bonds only, and domain (0,1) with singlets appearing on even bonds. Generalizing this concept to higher spins is straightforward: a spin- s site can be

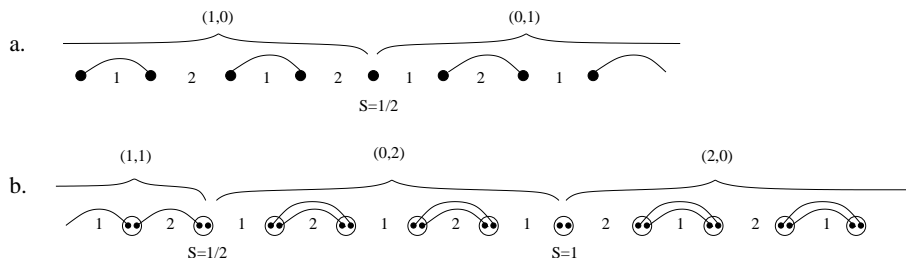


Figure 4. (a) Two domains are possible in the spin-1/2 Heisenberg model - (1,0) and (0,1). A domain wall between them gives rise to a spin 1/2 effective site. (b) In the case of a spin-1 chain, there are three possible domains: (1,1), (2,0), and (0,2), domain walls between them are effectively a spin-1/2 and spin-1 sites respectively.

represented as $2s$ spin-1/2 parts with a permutation symmetric wavefunction. The notation $(a, 2s - a)$ with $0 \leq a \leq 2s$ then signifies a domain with a spin-1/2 singlet links on odd bonds, and $2s - a$ spin-1/2 singlet links on even bonds. Each singlet link puts *one* of the spin-1/2 parts in neighboring sites in a singlet. Having a such singlet-links between two spin- s sites constrains their total spin to be $s_{total} \leq 2s - a$ [37].

This notation makes it easy to think about randomness as competition between different dimerizations. For each domain, there is a probability ρ_a to be of type $(a, 2s - a)$, and also, for each domain, there is a transfer matrix, which tells the probability of domain a to be followed by domain a' , which is $W_{aa'}$. Note that:

$$\sum_{a'=0}^{2s} W_{aa'} = 1.$$

At any finite temperature or energy scale, the non-frozen degrees of freedom (i.e., spins that were not yet decimated) lie on domain walls. Thus in the domain wall between the (1,0) and (0,1) domains, there is one free spin-1/2 site (see Fig. 4a). This free spin interacts with similar spin-1/2's in neighboring domain walls through an interaction mediated by quantum fluctuations of the domain in between. Thus each domain of type a is associated with a bond between neighboring free spins, and has a distribution of coupling $P_a(\beta)$, with β defined in Eq. (8).

The renormalization of strong bonds is now described as the decimation of domains. In the spin-1/2 chain, whenever a domain is decimated, its two neighboring domains, being identical, unite to form a single large domain; thus a singlet appears over the decimated domain, and connect the spins on the two domain walls. This is the Madhupata decimation step, Eq. (7). The random-singlet phase appears when the (1,0) and (0,1) domains have the same frequency. It is a critical point between the two possible dimerized phases associated with the two domains.

In $s > 1/2$ spin chains, the domain picture is richer. In the spin-1 Heisenberg chain there are three possible domains: (0,2), (1,1), and (2,0). The VBS is associated with the (1,1) phase, which has a uniform covering of the chain with spin-1/2 singlet links. On the other hand, the strong randomness random-singlet phase in this system occurs

when the competing domains are (2,0) and (0,2). This is completely analogous to the spin-1/2 random singlet phase, except that the domain walls consist of free spin-1 sites (see Fig. 4b).

A general domain wall between domains a and a' can be easily shown to have an effective spin:

$$S_e = \frac{1}{2}|a - a'| \quad (35)$$

as each singlet link leaving the domain wall removes a spin-1/2 from it.

Typically, the decimation of a domain involves forming as many singlet links as possible between the two domain walls. If the two neighboring domains are identical, $a' = a''$, then so are the domain walls, and a full singlet is formed; this is the Ma-Dasgupta decimation rule in Eq. (7). If the two domain walls are not identical, and interact with each other anti-ferromagnetically, singlet links forming between the two domain walls will exhaust one of the domain-wall spins, and the domain D_a will be swallowed by the domain containing the exhausted spin.

If the two domains neighboring a strong bond are different, $a' \neq a''$, and the interaction between the two domain-wall spins is ferromagnetic, the two spins unite into the domain wall between $D_{a'}$ and $D_{a''}$. For example, consider a (1,1) domain with an even number of links. it has to connect between a (2,0) domain and a (0,2) domain; both domain walls will have spin-1/2. Upon decimation of the (1,1) domain, we are left with a domain wall between (2,0) and (0,2), which has a spin-1.

Indeed at the critical point between the Haldane and random-singlet phases all three domains appear with equal probability—hence the designation “permutation-symmetric critical point”. Since each domain appears with the same frequency at the critical point, each possible domain wall appears with the same frequency as well. Two domain walls: (0, 2)–(1, 1) and (2, 0)–(1, 1) are effective spin-1/2’s, whereas the third possible domain wall, (2, 0)–(0, 2) is a spin-1. Thus, at any finite but low temperature or energy scale, 2/3 of the unfrozen degrees of freedom are effectively spin-1/2, and 1/3 are spin-1. These fractions are universal and a direct consequence of the bare spin of the model.

In general, each domain will have a logarithmic coupling strength β , and a distribution function $P_a(\beta)$. The flow equations for the transfer matrix probability $W_{aa'}$ are [32]:

$$\begin{aligned} \frac{dW_{aa'}}{d\Gamma} &= V_{aa'} - \frac{1}{2}W_{aa'}(P_a(0) + P'_a(0) - V_{aa} - V_{a'a'}) \\ V_{aa'} &= \sum_b W_{ab}P_b(\beta)W_{ba'} \end{aligned} \quad (36)$$

The flow equations of the distribution functions are:

$$\frac{dP_a(\beta)}{d\Gamma} = \frac{\partial dP_a(\beta)}{\partial d\beta} + P_a(0)P_a(\beta) + V_{aa} \left(P_a(\beta_1) \times P_a(\beta_2) - P_a(0) \right). \quad (37)$$

The perturbation symmetric fixed point solution of the above equations has all domains being equivalent: they appear with the same probability and have the same distribution function (note that this is only the fixed-point solution, and on the critical manifold the

bare system need not exhibit this symmetry; it is emergent). Eqs. (36, 37) are then solved by the attractive solution:

$$P_a(\beta) = \frac{2s}{\Gamma} e^{-2s\beta/\Gamma}, \quad (38)$$

$$\rho_a = \frac{1}{2s+1} \quad (39)$$

and:

$$W_{aa'} = \frac{1}{2s}(1 - \delta_{aa'}) = \frac{1}{2}(1 - \delta_{aa'}). \quad (40)$$

Eqs. (38-40) give a complete description of the spin- s critical point, and lead to the energy-length scaling properties, Eq. (18), of:

$$L \sim \frac{1}{\Gamma^{2s+1}}, \quad (41)$$

i.e.,

$$L^{1/(2s+1)} \sim \ln \Omega_0/\Omega. \quad (42)$$

For the spin-1 case, in particular, the permutation symmetric critical point describes the critical point between the Valence-Bond-Solid (VBS) Haldane phase, and the Random Singlet phase of a spin-1 Heisenberg chain.

2.4. Infinite-randomness fixed points of non-abelian anyons

Motivated by quantum Hall physics [38, 39, 40], and their possible application in topological qubits [41, 42, 43], the study of interacting non-abelian anyonic systems has moved to center stage. As non-abelian anyons are expected to appear as defects in quantum Hall states such as 5/2 or 12/5 [38, 39], it is natural to ask how a disordered system of such anyons behaves. The study of random non-abelian chains as started with the consideration of the random-singlet phase of Majorana fermions, and Fibonacci anyons [28, 44], and continued with the study of infinite randomness fixed points in the more general class of non-abelian chains, the truncated $SU(2)_k$ systems[45].

Non-abelian anyons are characterized first and foremost by fusion rules. A trivial example of a fusion rule in a simple abelian system is given by considering two spin-1/2's sites, which can fuse according to the the $SU(2)$ rule:

$$\frac{1}{2} \otimes \frac{1}{2} = 0 \oplus 1. \quad (43)$$

The random singlet phase of the AFM Heisenberg model arises when we always choose to fuse strongly interacting neighbors into the singlet (spin-0) state. For non-abelian anyons, the spin-compounding rule, Eq. (43) is substituted by the *fusion algebra* of the non-abelian system:

$$a \otimes b = \oplus \sum_c N_{ab}^c c, \quad (44)$$

where N_{ab}^c is the number of ways the superselection sectors a and b can fuse into c .

A major difference, however, between rules (43) and (44) is that fusion rules for a non-abelian algebra are always *closed*, while in regular spin-chains, the fusion rules include an infinite set of subspaces. The closure of the fusion rules results from the nonlocality of the Hilbert space of non-abelian systems. It implies that one can *always* apply a real-space RG scheme without ever generating new types of coupling in the renormalized Hamiltonian. Furthermore, just as in conventional spin chains, a decimation will result either in a Ma-Dasgupta renormalization of the neighboring couplings, or in their multiplication by a factor of magnitude smaller than 1. Therefore *sufficiently disordered (and most likely even weakly disordered) non-abelian chains will exhibit an infinite randomness behavior in the large length scale properties of their ground state*. Another counter-intuitive consequence of the fusion algebra, Eq. (44) is that the Hilbert space of individual non-abelian anyons (which are part of an interacting non-abelian system) can have non-integer dimension.

An important class of non-abelian anyons is the $SU(2)_k$ algebra, which arises in Read-Rezayi quantum Hall states that may describe fillings $\nu = n \pm k/(2 + k)$ [38]. This algebra is the truncated $SU(2)$ algebra, which allows two spins (corresponding to quasiparticles of the Read-Rezayi states) $s_1, s_2 \leq k/2$ to fuse into objects of total spin $s_{total} \leq k/2$. The fusion rule is then:

$$s_1 \otimes s_2 = |s_1 - s_2| \oplus \dots \oplus \min\{s_1 + s_2, k - s_1 - s_2\} \quad (45)$$

When $s_1 = s_2$, the two spins can fuse into the singlet state, i.e., the identity, $\mathbf{1}$.

Let us now consider a chain of N $SU(2)_k$ spin-1/2's. The dimension of the Hilbert space is given by $\dim H_N \approx d^N$ with

$$d = 2 \cos\left(\frac{\pi}{2 + k}\right). \quad (46)$$

The random Heisenberg AFM then has the form

$$\mathcal{H} = \sum_i J_i P_{i,i+1}^{\mathbf{1}}, \quad (47)$$

where $P_{i,i+1}^{\mathbf{1}}$ is the projection operator of two sites onto the identity subspace. When all couplings J_i are the same, the low energy behavior of the $SU(2)_k$ chain is described by a CFT with central charge $1 - 6/[(k + 1)(k + 2)]$. Clearly, when the J_i 's are random, this Hamiltonian is amenable to the Ma-Dasgupta decimation procedure. By applying second order perturbation theory using the F-matrix formalism of tensor categories, Bonesteel and Yang find that when two sites are bound into a singlet state, their neighbors interact with strength [28]:

$$J_{eff} = \frac{2}{d^2} \frac{J_L J_R}{J_m} \quad (48)$$

with $J_{L/R}$ are the couplings to the left and right of the decimated bond, whose strength is J_m . Since $2/d^2 < 1$, the $SU(2)_k$ Heisenberg model always flows to the random singlet fixed point, with arbitrarily weak randomness.

2.4.1. Majorana fermions. The simplest example of a random-singlet phase in a non abelian system occurs in a Majorana Fermion chain [28]. Majorana fermions, or real fermions, as they are sometimes called, can be constructed from fermion creation and annihilation operators, $\hat{\psi}^\dagger, \hat{\psi}$ [46]. We can construct two anti-commuting Majorana operators:

$$\sigma_1 = \hat{\psi}^\dagger + \hat{\psi} \quad \sigma_2 = i(\hat{\psi}^\dagger - \hat{\psi}) \quad (49)$$

note that $\{\sigma_i, \sigma_j\} = 2\delta_{ij}$, and that $\sigma_i = \sigma_i^\dagger$. Majorana fermions arise in the $SU(2)_2$ algebra, which also describes the CFT of the 2d Ising model. The fact that two Majorana fermions are required to form a fermionic state is reflected in the fusion algebra of $SU(2)_2$:

$$\sigma \otimes \sigma = \mathbf{1} \oplus \psi, \quad \psi \otimes \sigma = \sigma, \quad \psi \otimes \psi = \mathbf{1}. \quad (50)$$

ψ is a chiral fermionic state which arises when two σ 's are combined; it can either be occupied or empty. This double degeneracy of pairs of Majorana discloses their quantum dimension:

$$d = 2 \cos(\pi/4) = \sqrt{2}. \quad (51)$$

An $SU(2)_2$ Heisenberg chain consists of an array of σ , which are the spin-1/2, quasiparticles:

$$\mathcal{H} = \sum_j J_j i \sigma_j \sigma_{j+1}. \quad (52)$$

For the Ma-Dasgupta procedure, we need to find the eigenstates of a single bond, which is readily done by using Eq. (49):

$$\mathcal{H} = J_{2n} i \sigma_{2n} \sigma_{2n+1} = J_{2n} (2\hat{\psi}_n^\dagger \hat{\psi}_n - 1). \quad (53)$$

Thus, the ground state of the $2n$ bond corresponds to an empty fermionic state, and the excited state is the filled state. Using second order perturbation theory in conjunction with Eq. (49) yields Eq. (48), and the random singlet ground state of the Majorana chain.

It is instructive to note that by associating σ_{2n} and σ_{2n+1} with the fermionic state $\hat{\psi}_n$, we can rewrite Eq. (52) as:

$$\mathcal{H} = \sum_n \left[J_{2n} \left(\hat{\psi}_n^\dagger \hat{\psi}_n - \hat{\psi}_n \hat{\psi}_n^\dagger \right) + J_{2n+1} \left(\hat{\psi}_n \hat{\psi}_{n+1}^\dagger - \hat{\psi}_n^\dagger \hat{\psi}_{n+1} + \hat{\psi}_n \hat{\psi}_{n+1} - \hat{\psi}_n^\dagger \hat{\psi}_{n+1}^\dagger \right) \right]. \quad (54)$$

which is the Hamiltonian for the TFIM after a Wigner-Jordan transformation. Intuitively, the Jordan-Wigner transformation maps the Ising bonds into the fermionic states, and the transverse field into the odd bonds Majorana interaction, which results in hopping and pairing terms for the Fermionic states.

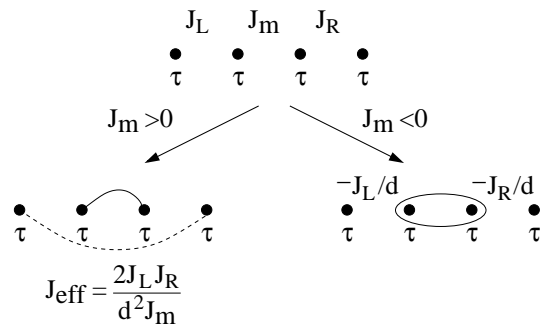


Figure 5. The two real-space RG steps in the Fibonacci chain. If $J_m > 0$, the Ma-Dasgupta AFM decimation of two τ 's leads to an AFM bond between the nearest neighbor, as Eq. (48) prescribes. In the FM case, where $J_m < 0$, two τ 's fuse and reverse the sign of the interaction of the fused τ with its neighbors [see Eq. (58)].

2.4.2. Fibonacci anyons. Fibonacci anyons arise in the $SU(2)_3$ algebra, which may describe the $\nu = 12/5$ quantum Hall state [38, 39]. These non-abelian anyons derive their name from the fusion algebra

$$\tau \otimes \tau = \mathbf{1} \oplus \tau. \quad (55)$$

If we consider a chain of N Fibonacci anyons, and ask how big is the Hilbert space they span, we can write for the combination of $n + 1$ particles: $d_{n+1} = d_{n-1} + d_n$, since whenever we combine another anyon it either forms a singlet with the topological charge, or another τ anyon. This recursion is solved by:

$$d_N \approx d^N = \left(\frac{1 + \sqrt{5}}{2}\right)^N, \quad (56)$$

i.e., the dimension d of Fibonacci anyons is the golden ratio.

The Fibonacci random Heisenberg model is identical to Eq. (47), but we can consider this model beyond the AFM model, by allowing J_i to be both positive and negative. This results in the FM/AFM Fibonacci model. A FM bond corresponds to a bond which is satisfied if the two anyons it connects fuse into another anyon, i.e., to the non-trivial fusion channel in rules (55):

$$J_i P_{i,i+1}^{\mathbf{1}} = -J(P_{i,i+1}^{\tau} - 1). \quad (57)$$

When addressing a random FM/AFM Fibonacci chain, we can still use the real-space decimation procedure, with the Ma-Dasgupta rule, Eq. (48) for AFM bonds, and with strong FM bonds renormalizing two sites into a single Fibonacci site: $\tau_i \otimes \tau_{i+1} = \tau_{i,i+1}$. By using the F-matrix rules for the Fibonacci anyons, we arrive at the surprising renormalization rules of neighboring bonds (see Ref. [44]):

$$J_{i\pm 1} \rightarrow -\frac{1}{d} J_{i\pm 1}, \quad (58)$$

where d is the golden ratio (see Fig. 5).

In order to find the fixed points of the Fibonacci anyons, we need to write flow equations for both FM and AFM bond distributions, which we denote $N(\beta)$ and $P(\beta)$ respectively. We obtain [44]:

$$\begin{aligned} \frac{dP}{d\Gamma} &= \frac{\partial P}{\partial \beta} + P(0) \left(P \overset{\beta}{\times} P + N \otimes N \right) + 2N(0)N(\beta) - N(0)P(\beta) \\ \frac{dN}{d\Gamma} &= \frac{\partial N}{\partial \beta} + 2P(0)N \overset{\beta}{\times} P - N(0)N(\beta) + 2N(0)P(\beta), \end{aligned} \quad (59)$$

where we again use the notation: $F \overset{x}{\times} G = \int_0^\infty dx_1 \int_0^\infty dx_2 \delta(x - x_1 - x_2) F(x_1) G(x_2)$. An exponential ansatz, $N(\beta) = n_0 e^{n_0 \beta / \Gamma}$, $P(\beta) = p_0 e^{p_0 \beta / \Gamma}$, for the fixed point distributions reveals two solutions. First, the pure AFM fixed point, which is just the random-singlet phase:

$$n_0 = 0 \quad p_0 = 1. \quad (60)$$

But a second fixed point is found by

$$p_0 = n_0 = 1. \quad (61)$$

This fixed point has an equal proportion of FM and AFM bonds, and although it is an infinite-randomness fixed point, with coupling distributions:

$$N(\beta) = P(\beta) = \frac{1}{\Gamma} e^{-2\beta/\Gamma}. \quad (62)$$

This new fixed point belongs to the spin-1 Damle-Huse universality class, which describes the three-domain permutation symmetric fixed point between the Haldane phase and the random singlet phase in a random spin-1 Heisenberg chain [32, 36, 35].

Surprisingly, a stability analysis reveals that the random singlet fixed point is actually unstable to flow to the FM/AFM mixed fixed point. This is a consequence of the FM decimation step, Eq. (58), which allows a single FM bond to shift two neighboring AFM bonds to FM upon decimation. A reasonable conjecture is that the pure FM Fibonacci chain flows to the infinite-randomness mixed FM/AFM fixed point upon disordering of the couplings J_i 's. The pure FM fixed point is described by a CFT with central charge $c = 4/5$ [47, 48].

Another note is that the mixed FM/AFM random Heisenberg chain for $SU(2)$ spin-1/2's was studied in Refs. [49, 50]). Within the real-space RG approach it is easy to see that higher and higher spins are generated, and as a result, the model has a *finite* randomness fixed point which was observed numerically.

2.4.3. General $SU(2)_k$ models. From the Fibonacci example it is easy to see how we can obtain different Heisenberg models which are not purely AFM for any $SU(2)_k$ models. For k odd, it was shown in Ref. [45] that all fixed points arising in these models (i.e., nearest neighbor random chains) are indeed infinite randomness fixed points. A bit disappointingly, all of these fixed points belong to the Damle-Huse hierarchy; the permutation symmetric points of spin- s Heisenberg models are realized in $k = 2s + 1$

truncated $SU(2)_k$ models; some intuition to this relationship is that the types of non-abelian anyons are mapped into domains in the spin-models. The topological properties of the $SU(2)_k$ algebra, however, guarantee that the Damle-Huse points are stable fixed points, and therefore describe *phases* rather than critical points. This indeed fits our finding of the mixed FM/AFM fixed point of the Fibonacci chain ($k = 3$) being stable, and corresponding to the $s = 1$ Damle-Huse fixed point.

2.5. Generalized transverse field models

A model that played an important role in the study and understanding of the entanglement entropy of random spin chains is the generalized random transverse field model (GTFIM) introduced by Santachiara [51]. Each site in the N -flavor GTFIM has N states, $\{|q\rangle\}_{q=1}^N$. The Hamiltonian for this model is:

$$\mathcal{H}_N = - \sum_i J_i \sum_{n=1}^{N-1} \alpha_n (S_i^{z\dagger} S_{i+1}^z)^n - \sum_i h_i \sum_{n=1}^{N-1} \alpha_n \Gamma_i^n \quad (63)$$

with:

$$S_i^z |q\rangle_i = e^{2\pi i q/N} |q\rangle_i, \Gamma_i = \sum_{q=1}^N (|q\rangle_{i,i} \langle q+1| + |q+1\rangle_{i,i} \langle q|) \quad (64)$$

with $|N+1\rangle = |1\rangle$. The coefficients $\alpha_n \geq 0$ obey $\alpha_n = \alpha_{N-n}$ to maintain hermiticity of the model.

To carry out a real space RG analysis we need to find the eigenstates of the local operators in the Hamiltonian (63). The eigenstates of the $S_i^z S_{i+1}^z$ term in this Hamiltonian are of the type:

$$|q, \Delta q\rangle_{i,i+1} = |q\rangle_i |q + \Delta q\rangle_{i+1} \quad (65)$$

with energies:

$$E_{\Delta q}^{zz} = - \sum_{n=1}^{N-1} \alpha_n \cos(2\pi n \Delta q/N) \quad (66)$$

with the ground states being N times degenerate, $|q, \Delta q = 0\rangle_{i,i+1} = |q\rangle_i |q\rangle_{i+1}$. The eigenstates of the Γ_i term are:

$$|p\rangle_i = \sum_{q=1}^N e^{2\pi i p/N} |q\rangle_i \quad (67)$$

with energies:

$$E_p^\Gamma = - \sum_{n=1}^{N-1} \alpha_n \cos(2\pi n p/N). \quad (68)$$

The fact that the spectrum of the $S^z S^z$ and Γ terms is identical is a reflection of a duality which the GTFIM possesses.

Let us go to the decimation procedure for the case of a strong J and h . When encountering a strong $J_i = \Omega$, we set $q_i = q_j = q$ to form the $|q, \Delta q = 0\rangle_{i,i+1}$ eigenstate.

This eigenstate is N times degenerate. The degeneracy between the various q states is lifted through the action of the Γ_i and Γ_{i+1} terms, which in second order perturbation theory form an effective term:

$$\mathcal{H}_{i,i+1} = \frac{h_i h_{i+1}}{\kappa_1 \Omega} \sum_{n=1}^{N-1} \tilde{\alpha}_n \Gamma_{i,i+1}^n \quad (69)$$

with:

$$\begin{aligned} \kappa_n &= \frac{1}{2} \sum_{m=1}^{N-1} \alpha_m (\cos(2\pi mn/N) - 1) \\ \tilde{\alpha}_n &= \alpha_n^2 \frac{\kappa_1}{\kappa_n}. \end{aligned} \quad (70)$$

The decimation step for a strong $h_i = \Omega$ entails setting site i into the state $|p=0\rangle_i = \sum_{q=1}^N |q\rangle_i$. Through a second order process, the bonds to the left and right of the decimated site induce an effective interaction:

$$\mathcal{H}_{i-1,i+1} = \frac{J_{i-1} J_i}{\kappa_1 \Omega} \sum_{n=1}^{N-1} \tilde{\alpha}_n (S_{i-1}^z \dagger S_{i+1}^z)^n \quad (71)$$

with κ_n and $\tilde{\alpha}_n$ following Eq. (70).

The discussion above was completely general, and did not depend on the actual values of α_n . Therefore, under the condition that $\alpha_n \leq 1$, regardless of the choice of $\{\alpha_n\}$, a GTFIM also flows to an infinite randomness fixed point, with the same universal properties as the TFIM, but with a site degeneracy of N rather than 2.

An important realization of the GTFIM has the following choice of $\{\alpha_n\}$:

$$\alpha_n = \frac{\sin(\pi/N)}{\sin(\pi n/N)}. \quad (72)$$

With this choice of α_n , the critical ($J = h$) pure GTFIM coincides with the parafermionic Z_N CFT, which has central charge:

$$c_N = 2 \frac{N-1}{N+2}. \quad (73)$$

Upon allowing J_i and h_i vary randomly at each site, we can apply RSRG to this model as well. After a few application of the renormalization rules, and Eq. (70) in particular, the set $\{\alpha_n\}$ renormalizes to:

$$\tilde{\alpha}_n = \delta_{1,n}, \quad (74)$$

which coincides with the Z_N clock model. This model was analyzed in Ref. [52] and was shown to flow to strong randomness as anticipated above.

3. Entanglement entropy in infinite-randomness fixed points

3.1. Spin-1/2 random singlet entanglement entropy

The simplest case for computing the entanglement entropy is the random singlet phase of the spin-1/2 Heisenberg model. The entanglement entropy of a spin-1/2 particle in a

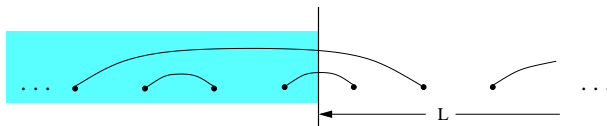


Figure 6. The entanglement entropy of a segment is the number of singlets that connect the segment with the rest of the chain (shaded area). In this example there are two such singlets.

singlet with another such particle is 1 (bit), which is the entropy of a spin (e.g. a) in a singlet, $|\psi\rangle = \frac{1}{\sqrt{2}}(|\uparrow\rangle_a |\downarrow\rangle_b - |\downarrow\rangle_a |\uparrow\rangle_b)$ with its partner, b , traced out. The entanglement of a segment of the random Heisenberg chain is just *the number of singlets that connect sites inside to sites outside the segment* (Fig. 6).

To obtain the entanglement, we calculate the number, N , of singlets that form over a single bond B up to the length-scale L . A quick argument shows that the entanglement should scale logarithmically with the length L . If we neglect the history dependence of the distribution of bond B , we can find N by using the distribution of bond strengths, Eq. (14). The probability of a singlet forming across the bond B when we change the energy scale $\Omega \rightarrow \Omega - d\Omega$, $\Gamma \rightarrow \Gamma + d\Gamma$ is also the average number of singlets forming. It is given by:

$$d\bar{N} = d\Gamma P(\beta = 0) = \frac{d\Gamma}{\Gamma} \quad (75)$$

integrating this leads to $\bar{N} = \ln \Gamma \approx \frac{1}{2} \ln L$ if we stop counting at length scale $L \sim \Gamma^2$.

Taking into account that the entanglement of a segment of length L with the rest of the chain has two ends, we get:

$$S_L \sim N_L \approx 2 \cdot \ln \sqrt{L} + k = \ln L + k, \quad (76)$$

where k is a non-universal constant, which also depends on the initial realization of the disorder.

The history of singlet formations over B is required to get the correct coefficient of $\ln L$ in Eq. (76). From Eq. (76) we see that singlets form at a constant rate with respect to an 'RG time' $\ell = \ln \Gamma$. Quite generally, we can define the average RG time between Ma-Dasgupta decimations as $\bar{\ell} = \overline{\ln \Gamma_1 - \ln \Gamma_0}$, where Γ_0 and Γ_1 are the RG scales at consecutive singlet formations. We can write the following general formula:

$$S_L \sim \frac{1}{3} c_{eff} \log_2 L = 2 \frac{\ln \Gamma_L}{\bar{\ell}} \bar{S}_{total}, \quad (77)$$

where $\ln \Gamma_L$ is the total 'RG time' for a segment of length L , and S_{total} is the average entanglement per Ma-Dasgupta decimation, which in the Heisenberg model is simply singlet formation, $\bar{S}_{total} = 1$.

Next, we find $\bar{\ell}$ in the random singlet phase. Right after a Ma-Dasgupta decimation step occurs, the resulting bond is strongly suppressed (see Eq. (7)); the initial bond strength distribution of an effective bond forming over a decimated bond at Γ_0 is

$$Q(\beta) = \int d\beta_1 d\beta_2 \delta_{(\beta_1 + \beta_2 - \beta)} P_{\Gamma_0}(\beta_2) P_{\Gamma_0}(\beta_1) = \frac{\beta}{\Gamma_0^2} e^{-\beta/\Gamma_0}. \quad (78)$$

As the RG progresses, this distribution evolves as $Q_\Gamma(\beta)$ with the following evolution equation:

$$\frac{dQ_\Gamma(\beta)}{d\Gamma} = \frac{\partial Q_\Gamma(\beta)}{\partial \beta} - 2Q_\Gamma(\beta)P_\Gamma(0) + 2P_\Gamma(0)P_\Gamma \times Q_\Gamma. \quad (79)$$

which is literally what happens when the bond B is next to a decimated bond. The first term is due to the change in β when Ω changes, the second and third terms account for B 's flow due to one of its two neighbors forming a singlet. Note that $\frac{dp_\Gamma}{d\Gamma} = -Q_\Gamma(0)$. Eq. (79) can be solved using the ansatz:

$$Q_\Gamma(\beta) = \left(a_\Gamma + b_\Gamma \frac{\beta}{\Gamma} \right) P_\Gamma(\beta) \quad (80)$$

by substituting Eq. (80) in Eq. (79) we obtain

$$\frac{da_\Gamma}{d\Gamma} = b_\Gamma - 2a_\Gamma, \quad \frac{db_\Gamma}{d\Gamma} = -b_\Gamma + a_\Gamma, \quad (81)$$

with $l = \ln \Gamma / \Gamma_0$. Also $a_{\Gamma_0} = 0$, $b_{\Gamma_0} = 1$, from Eq. (78).

Now, the probability the the bond B was not decimated again is given by: $\int_0^\infty d\beta Q_\Gamma(\beta) = p_\Gamma = a_\Gamma + b_\Gamma$ and depends on Γ *only through* $l = \ln \Gamma / \Gamma_0$, reaffirming our definition of 'RG time' ℓ . We find:

$$\bar{\ell} = \int dp_\Gamma \ell = \int_0^\infty d\ell a_\Gamma \ell. \quad (82)$$

From Eq. (81) one finds

$$a_\Gamma = \frac{1}{\sqrt{5}} \left(e^{-\frac{3-\sqrt{5}}{2}\ell} - e^{-\frac{3+\sqrt{5}}{2}\ell} \right), \quad (83)$$

$$b_\Gamma = \frac{1}{2} \left[\left(1 + \frac{1}{\sqrt{5}} \right) e^{-\frac{3-\sqrt{5}}{2}\ell} - \left(1 - \frac{1}{\sqrt{5}} \right) e^{-\frac{3+\sqrt{5}}{2}\ell} \right].$$

Inserting this in Eq. (82) we find $\bar{\ell} = 3$. Therefore:

$$S_L = \frac{1}{3} \cdot 2 \ln \Gamma + k = \frac{\ln 2}{3} \log_2 L + k. \quad (84)$$

Hence the 'effective central charge' of the random Heisenberg chain is $\tilde{c} = 1 \cdot \ln 2$, which is the central charge of the pure Heisenberg chain times an irrational number: $\ln 2$.

The same analysis precisely applies to an easy-plane XXZ chain, since its ground state is also a random singlet fixed point.[53] This model also has $c = 1$ in the pure case, and a reduced effective central charge, $c_{eff} = 1 \cdot \ln 2$, in the random case.

3.2. General formula for random singlet phases

Now that we have calculated the entanglement entropy of the spin-1/2 random singlet phase, we can easily calculate the entanglement of any random singlet phase, so long as we know what is the von-Neumann entropy encapsulated in each site in the system.

In a random singlet phase of a system of sites with a local Hilbert space dimension D , we would then have [28]:

$$S_L = \frac{1}{3} \ln L \log_2 D = \frac{1}{3} \ln D \log_2 L. \quad (85)$$

For example, the bipartite entanglement in a spin- S random singlet phase (where strong bonds put pairs of sites into the zero total spin state) is $S_L = \frac{1}{3} \ln(2S + 1) \log_2 L$ [54].

A sufficient condition for the entanglement per singlet to be $\log_2 D$ is that the local Hilbert space is a D -dimensional irreducible representation of some symmetry group, and that the singlet that two sites form is the zero-dimensional representation of the group. Under these conditions, when we look at the density matrix of such two sites, and trace over one of them, the reduced density matrix, $\hat{\rho}_{red}$ is a D dimensional matrix, which must commute with all group elements, $\hat{g}\hat{\rho}_{red} = \hat{\rho}_{red}\hat{g}$, and therefore by Schor's lemma it must be:

$$\hat{\rho}_{red} = I/D \quad (86)$$

with I being the identity matrix. The von Neumann entropy is then $-\text{tr} \hat{\rho}_{red} \log_2 \hat{\rho}_{red} = \log_2 D$. The above arguments would apply also to random $SU(N)$ antiferromagnetic spin-chains, investigated by Hoyos and Miranda [55].

3.3. Non-abelian random singlet phases

In Sec. 2.4 we reviewed the unique random singlet phases of non-abelian anyons. The entanglement entropy of these phases follows the general formula (85), but with the dimension D now being the *quantum dimension* of each site. A rigorous way to prove this is given in Refs. [28, 44]. A simple way of anticipating the answer, however, is to notice that the Hilbert space of N sites, each containing a non-abelian charge a with quantum dimension D , will have a Hilbert space of dimension:

$$\dim \mathcal{H}^N \rightarrow D^N \quad (87)$$

as $N \rightarrow \infty$. Since the entanglement entropy of a segment L in a chain is accumulated from many singlets forming over the partition bond, connecting the inside of the segment with its complement, the entanglement per singlet is essentially the log of the Hilbert space of all the sites on one side of the partition.

Specific examples are the entanglement of the Majorana chain's random singlet phase of Ref. [28], where $D = \sqrt{2}$, and the bipartite entropy is:

$$S_{Majorana} = \frac{1}{3} \cdot \frac{1}{2} \ln 2 \log_2 L \quad (88)$$

and the Fibonacci anyon random singlet case, where the quantum dimension D is the golden mean, $\tau = \frac{1}{2}(1 + \sqrt{5})$, with entanglement:[28]

$$S_{Fibonacci} = \frac{1}{3} \ln \tau \log_2 L = \frac{1}{3} (0.481211 \dots) \log_2 L. \quad (89)$$

3.4. Transverse field Ising model

The critical point of the random TFIM has the same universal infinite-randomness scaling as the Heisenberg model. The distributions of the Ising couplings and the transverse fields are the same. When considering the entanglement entropy between two segments connected by the bond B , however, if the Ising coupling at B is decimated,

the boundary of the segment becomes a site, with a transverse field distribution given by Eq. (80) and (83). Entanglement only occurs once the site straddling the segment boundary is decimated. After the decimation, the part of the cluster to the right of the partition becomes a mixed state, and contributes $\bar{S}_{h-dec} = \log_2 2 = 1$ entropy. Following the boundary-*site* decimation the process repeats, and entanglement accumulates

Thus instead of obtaining entropy 1 per Ma-Dasgupta decimation, we only obtain entropy every second Ma-Dasgupta decimation. Referring back to our general formula for entanglement entropy, Eq. (77), we have $\bar{\ell} = 3$, as before, but the average entanglement per Ma-Dasgupta decimation is $\bar{S}_{total} = 1/2$. Thus:

$$S_L = \frac{1}{6} \ln L + k = \frac{\ln 2}{6} \log_2 L + k, \quad (90)$$

with k a non-universal constant. The effective central charge of the random quantum Ising model is $\tilde{c} = 1/2 \cdot \ln 2 - \ln 2$ times the central charge of the pure system.

3.5. Generalized TFIM and pure-random c increase

The xxz, Heisenberg and TFIM all seem to have their effective central charge reduce as they flow from the pure CFT fixed point, to the infinite randomness fixed point. Santachiara, however, demonstrated that this is not the rule using the generalized TFIM described in Sec. 63 above.

The calculation of the entanglement entropy for the random GTFIM is identical to the that of the random TFIM, with one exception: the state of the site straddling the partition is, quite generally,

$$|B\rangle = \sum_{q=1}^N |q\rangle_L |q\rangle_R. \quad (91)$$

Therefore upon decimation, the entanglement that results is $\log_2 N$. Since this entanglement is added only every site-decimation, and not bond decimation, the average entanglement per Ma-Dasgupta decimation is $\bar{S}_{total} = \frac{1}{2} \log_2 N$, and the total entanglement is:

$$S_L = \frac{1}{6} \log_2 N \ln L + k = \frac{\ln N}{6} \log_2 L + k, \quad (92)$$

i.e., it has:

$$c_{eff}^{(N)} = \ln \sqrt{N}. \quad (93)$$

When $N \geq 42$, $c_{eff}^{(N)} > c_N$, which means that as the pure parafermionic Z_N CFT flows to the infinite randomness fixed point, its entanglement entropy increases, ruling out a pure-random c -theorem.

3.6. Entanglement entropy of infinite randomness fixed points beyond random singlet.

As explained in the introduction, there is a hierarchy of infinite-randomness fixed points with the Damle-Huse exponents $\psi = 1/(2s + 1)$ and $\chi = 2s$. The calculation of

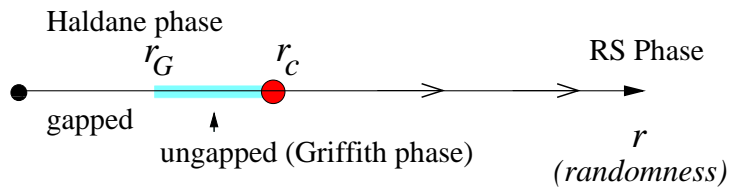


Figure 7. Phase diagram of the spin-1 random Heisenberg model. At no disorder, $r = 0$, the chain is in the gapped Haldane phase and its ground state resembles a valence-bond solid (VBS). As randomness is increased, the gap is destroyed at r_G , but the VBS structure survives up to the critical point, $r = r_c$. At $r > r_c$ the chain is in the spin-1 random-singlet phase. At the critical point, the spin-1 permutation symmetric Damsle-Huse fixed point obtains, which has $\psi = 1/2$, and $\chi = 2$ [32, 35, 36]. The Entanglement entropy calculation finds that at the permutation symmetric point $c_{eff}^{(r_c)} = 1.232$, and at the random singlet fixed point $c_{eff}^{s=1RS} = \ln 3 = 1.099$.

entanglement entropy in non-random singlet fixed points requires an understanding of the complicated structures that arise in the quantum state of such points, and the various Ma-Dasgupta decimations that are possible. For instance, in the case of a spin-1 permutation-symmetric fixed point (Sec. 4), Ma-Dasgupta decimation of a (2,0) domain lying between two (1,1) domains is different than Ma-Dasgupta decimation of a (1,1) domain between two (0,2) domains. Similarly, the domain walls have an internal structure which arises from non-Ma-Dasgupta decimations, e.g., a ferromagnetic decimation of a (1,1) domain lying between a (0,2) domain on one side, and a (2,0) domain on the other.

The strategy for addressing the more complex history dependence is to revisit the formulation of the entanglement formula, Eq. (77), but allowing for different Ma-Dasgupta decimation configurations:

$$S_L \sim \frac{1}{3} c_{eff} \log_2 L = 2 \frac{\ln L^\psi}{\sum_c p_c \bar{\ell}_c} \sum_c (p_c \bar{S}_c). \quad (94)$$

The sum over c goes over all possible configurations of the quantum state at the partition bond at a Ma-Dasgupta decimation. $\bar{\ell}_c$ is the average RG time for the configuration c to form, and \bar{S}_c is the entanglement entropy of the configuration.

Without going into details, let us review results for the spin-1 phase diagram, and for the Fibonacci anyon phase diagram.

3.6.1. Spin-1 entanglement entropy. The phase diagram of the spin-1 Heisenberg chain is given in Fig. 7. In Ref. [53] we calculated the entanglement entropy of the permutation symmetric fixed point using the method described above. We found that the leading contribution to the entanglement entropy of the spin-1 random Heisenberg model at the Haldane-RS critical point is:

$$S \sim \frac{1}{3} c_{eff} \log_2 L = \frac{1}{3} \frac{4}{3} \cdot (1.3327 - 10^{-3}) \cdot \ln 2 \log_2 L. \quad (95)$$

where the subtraction indicates the uncertainty in the results, which is an upper bound. The effective central-charge we find is thus:

$$c_{eff}^{(rc)} = 1.232 \quad (96)$$

This effective central charge is smaller than that of the pure system at the corresponding critical point, $c_{eff}^{rc} < 3/2$. This effective central charge is also bigger than the effective central-charges of both the Haldane phase, which vanishes, and the spin-1 RS phase, which has:

$$c_{eff}^{s=1 RS} = \ln 3 = 1.099. \quad (97)$$

Thus in the case of the spin-1 chain, the effective central charge drops both along flow lines between the pure and random fixed points, as well as between different infinite randomness fixed points.

3.6.2. Fibonacci chains entanglement entropy The random Fibonacci chain's phase diagram is split between two infinite randomness phases. The AFM Heisenberg model flows to the random-singlet phase, while any density of 'ferromagnetic couplings', which prefer nearest-neighbors fusing in the τ channel, destabilizes the random singlet phase, and makes the chain flow to a mixed infinite-randomness phase, which is in the same universality class as the Damle-Huse permutation symmetric fixed point for spin-1.

The entanglement entropy of a segment of length L in the random singlet phase of the Fibonacci chain is easily found in Eq. (89); the effective central charge in this phase is $c_{eff}^{RS} = \ln \frac{1+\sqrt{5}}{2} = 0.481211\dots$. By summing up the contributions of various fusion configurations between Ma-Dasgupta decimations, and the RG time they require to form, we find the entanglement entropy of a chain segment with length L in the mixed FM/AFM phase to be: [44]

$$S \sim \frac{1}{3}c_{eff} \log_2 L = \frac{1}{3}0.702 \log_2 L, \quad (98)$$

i.e., the effective central charge is $c_{eff}^{mixed} = 0.702$.

It is hard to provide intuition for this result. Nevertheless, it is interesting to compare it with its pure-system analog, and to the effective central charge of the random singlet phase. It is most likely that the mixed IR phase is also the terminus of flow from the ferromagnetic pure Fibonacci chain. The central charge of the critical FM golden chains was determined in Ref. [47] to be $c = 4/5 = 0.8 > c_{eff}^{mixed}$. Hence the effective central charge dropped along the flow. Comparing our result, though, to the central charge in the random singlet phase immediately reveals that the effective central charge *increased* in the strong-randomness RG flow from the random singlet phase to the mixed IR phase. Thus the suggestion that strong-randomness flows may have a c-theorem associated with them is contradicted.

Note that by considering the central charges of the of the two critical phases of the pure chain, $c^{AFM} = 0.7$, and $c^{FM} = 0.8$, we find that by the Zamolodchikov c-theorem,[17] the AFM phase must be stable against FM bond introduction, unless

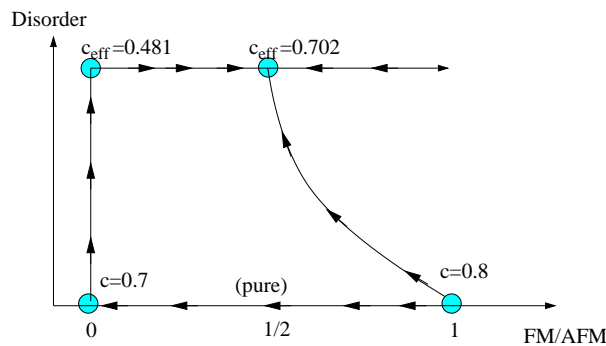


Figure 8. Flow diagram of the pure and disordered golden chain. In the pure chain, assuming no intervening fixed points exist, the FM fixed point is unstable to flow to the AFM fixed point, as inferred from the Zamolodchikov c -theorem. In the disordered chain, however, the flow is in the opposite direction, with the mixed FM/AFM phase, which is most likely the terminus of the flow from the pure FM phase, being stable relative to the random singlet phase, which is the result of disordering the pure AFM phase. The fixed point (effective) central charges are also quoted.

another critical point appears in between, which we speculate is unlikely. The flow in the random Fibonacci chain, however, is the opposite: the mixed FM/AFM phase is stable for essentially all chain coupling distribution, except for the solely antiferromagnetic point. This situation and our results are summarized in Fig. 8.

4. Towards measurements of entanglement entropy

4.1. Measurement entropy and bounds on entanglement entropy

The study of entanglement entropy of interacting systems suffers from the fact that it is an abstract quantity which is not easy to measure. Indication that entanglement exists could be found by confirming Bell inequalities [56, 57]. Formally, a theory of entanglement witnesses has been developed [58, 59, 60], but these seem still specific to two particle systems, and does not provide a quantitative measure of entanglement.

More recently, the connection of bipartite entanglement and measurement noise was explored as a way of quantifying entanglement entropy [7, 61, 62]. We define "measurement entropy" of an observable \hat{O} , as the Shannon entropy $S[\hat{O}] = -\sum_x P(x) \log P(x)$ associated with the probability distribution $P(x)$ of the outcomes x of \hat{O} [63]. In classical systems this quantity, measurable by definition, is always lower than the overall entropy. However, in quantum systems it can in general be either larger or smaller than the entanglement entropy \bar{S} . If we consider measurements of local operators as described below, we can prove that their measurement entropy provides a lower bound on entanglement.

Given a state ψ of interest, we denote by \mathcal{L} the set of observables $\hat{O} = \hat{O}_A \otimes I + I \otimes \hat{O}_B$. Nevertheless even for observables for which the measurement entropy is larger than the Von Neuman entropy, information can still be gained in the measurement [63]

\hat{O}_B , acting locally on A and B , for which ψ is an eigenstate. Let us write the Schmidt decomposition of ψ as $\psi = \sum c_i^\alpha |\alpha, i\rangle \otimes |s-\alpha, i\rangle$, where s is the eigenvalue of \hat{O} acting on ψ , and such that $\hat{O}_A |\alpha, i\rangle = \alpha |\alpha, i\rangle$ and $\hat{O}_B |s-\alpha, i\rangle = (s-\alpha) |s-\alpha, i\rangle$ (here i ranges over the degeneracy of eigenstates of \hat{O}_A with value α). The reduced density matrix can now be written as $\rho_A = \text{tr}_B \rho = \sum P_\alpha \rho_\alpha$, where we have defined $\rho_\alpha = \frac{1}{P_\alpha} \sum |c_i^\alpha|^2 |\alpha, i\rangle \langle \alpha, i|$ and $P_\alpha = \sum_i |c_i^\alpha|^2$ is the measurement outcome distribution. For the entanglement entropy we have in this case:

$$\mathcal{S}_E = S[\hat{O}_A] - \sum P_\alpha \text{tr} \rho_\alpha \log \rho_\alpha \geq S[\hat{O}_A]. \quad (99)$$

where $S[\hat{O}_A]$ is the measurement entropy associated to the probability distribution P_α . This inequality in Eq. (99) is completely general. Interestingly, the equality $\mathcal{S}_E = S[\hat{O}_A]$ is realized either if all α outcomes are non-degenerate, or when the ρ_α 's describe pure states. The bound (99) becomes better and better by choosing a set of commuting operators \hat{O} such that all the degeneracy in the measurement result α is removed.

"Conserved" operators are natural candidates for the local operators we denote \mathcal{L} above, i.e. sums of local operators which commute with the Hamiltonian of the system. For instance, consider the total spin operator for spin chains with rotational symmetry. Generally, the best choice of \hat{O} requires a more elaborate analysis.

4.2. Entanglement measurement in the random singlet phase

Bipartite entanglement and fluctuations of a conserved quantity have a particularly close relationship in the random singlet phase of the spin-1/2 easy-plane xxz and Heisenberg chains. The Hamiltonian (20) only commutes with $\hat{S}_{total}^z = \sum_i \hat{S}_i^z$ (note, however, that its ground state has a full rotational symmetry). Therefore $\hat{S}_A = \sum_{i \in A} \hat{S}_i^z$ is the operator of choice for estimating the entanglement between part A and the rest of the chain. In the random singlet phase there are two types of singlets: (a) N_{AB} singlets connecting between A and B , (b) $N_{AA} + N_{BB}$ singlets connecting sites in A to other sites in A , or sites in B to other sites in B . As explained in Sec. 3.1, each singlet contributes 1 to the entanglement entropy, and therefore: $\mathcal{S}_E = N_{AB}$. But in addition, each singlet contributes 1/4 to the variance of the measurement of \hat{S}_A . Therefore, the random-singlet phase entropy not only obeys Eq. (99), but can be completely measured by the relation:

$$\mathcal{S}_E = 4 \langle \Delta(\hat{S}_A^z)^2 \rangle = N_{AB}. \quad (100)$$

One possible design for an entanglement measurement through the variance of \hat{S}_A^z is to use a SQUID with a well defined flux-pickup region, interacting with a Heisenberg chain realized using solid-state spins (see, e.g., [64, 65]). A SQUID that couples, and can measure, the magnetic flux of electronic spins in part of the chain, essentially carries out a measurement of \hat{S}_A^z , where A is the region of measurement. Recent measurements of flux qubits have shown that they are very sensitive to localized two level systems in their vicinity [66, 67]; these two-level systems were conjectured to be electronic spins in Ref. [68, 65].

5. Anderson localization

5.1. Localization and multifractality

When quantum particles encounter a spatially random potential, their wave function may become localized; this is the well known phenomenon of Anderson localization [69]. To be specific, consider the following random on-site potential problem:

$$\mathcal{H} = - \sum_{\langle ij \rangle} t c_i^\dagger c_j + \sum_i V_i c_i^\dagger c_i \quad (101)$$

with the on-site potential randomly distributed in the range $-W/2 \leq V_i \leq W/2$. At high values of the disorder width, W/t , all eigenfunctions of (101) are localized. Following [70], in 3d, when W/t reaches the critical value $w_c = 16.3$, delocalized states begin to appear in the middle of the band. As W/t decreases further, the mobility edge between localized and delocalized states moves away from the center of the band, and eventually reaches the bottom (and top) of the band so that all states are localized.

Apart from major implications for transport properties, the Anderson localization transition (as a function of single-particle energy, i.e., chemical potential) is associated with universal behavior reflected in the wave function properties. In particular, a localized wave function at energy $E < E_c$, where $E_c < 0$ is the energy at the mobility threshold, has a localization length which behaves as:

$$\xi \sim \frac{1}{|E - E_c|^\nu}. \quad (102)$$

The wavefunction actually exhibits an even richer universal behavior which is expressed by its *multifractality*. Consider the integral of the wavefunction raised to some power $2q$ over all space. This has a nontrivial universal dependence on the system size:

$$P_q(E) = \sum_i |\psi_i|^{2q} \sim \frac{1}{L^{\tau_q}} \mathcal{F}_q(L^{1/\nu}(E_c - E)). \quad (103)$$

This form is quite general for Anderson localized systems, with τ_q and ν depending on the universality class of the problem [71]. For the model Eq. (101), in three dimensions, it was found that $\nu = 1.57 \pm 0.03$ [72]. In the case of a pure system, we have $|\psi_i|^{2q} = L^{d(q-1)}$, where d is the dimensionality of the system.

5.2. Single site entanglement entropy and localization

One measure of entanglement entropy of a wave function is the average single-site entanglement. This measure can be used to characterize single-particle wave functions, and it differs from the many-body bipartite entanglement entropy used above. Its usefulness is also in its universal properties at critical points [73]. This is true for Anderson-type localization transitions as well, as was shown in [74], which we review briefly here.

The average single site entanglement is defined as follows. Write the wave function as:

$$|\psi\rangle = \sum_i \psi_i |1\rangle_i \prod_{j \neq i} |0\rangle_j \quad (104)$$

where $|n\rangle_i$ indicates n particles at site i . It is easy to see that the reduced density matrix, obtained by tracing over all occupations of sites *except* i , is

$$\rho_i^{red} = |\psi_i|^2 |1\rangle_i \langle 1| + (1 - |\psi_i|^2) |0\rangle_i \langle 0|. \quad (105)$$

Thus the entanglement between site i and the rest of the system is:

$$S_i = -|\psi_i|^2 \ln(|\psi_i|^2) - (1 - |\psi_i|^2) \ln(1 - |\psi_i|^2). \quad (106)$$

Anticipating that the wave function is localized over a number of sites, $\ell \gg 1$, we have $|\psi_i|^2 \ll 1$. Therefore we can neglect the second term above, yielding:

$$\overline{S}_{ss} = \overline{S}_i \approx -\frac{1}{L^D} \sum_i |\psi_i|^2 \ln(|\psi_i|^2). \quad (107)$$

The scaling properties of the average single-site entanglement for wave functions with energy E can be obtained from the multifractal spectrum above:

$$\overline{S}_{ss}(E) = \left. \frac{\partial P_q(E)}{\partial q} \right|_{q \rightarrow 1} = \ln LP_q(E) \cdot \left. \frac{\partial \tau_q}{\partial q} \right|_{q \rightarrow 1} + \left. \frac{1}{L^{\tau_q}} \frac{\partial \mathcal{F}_q}{\partial q} \right|_{q \rightarrow 1} \quad (108)$$

At criticality this will reduce to:

$$\overline{S}_{ss}(E_c) \sim \alpha_1 \ln L. \quad (109)$$

A metal, or a pure system, would just have $P_q(E) \sim L^{D(q-1)}$, and therefore:

$$\overline{S}_{ss}^{metal} \sim DL^{D(q-1)} \ln L. \quad (110)$$

Both limits seem to indicate that the first term in Eq. (108) dominates. Therefore we conclude that the single site average entanglement in the vicinity of Anderson transitions is:

$$\overline{S}_{ss}(E) = \ln LK(L^{1/\nu}(E - E_c)). \quad (111)$$

6. Numerical studies

The strongly random quantum critical points that are the main focus of this review can be studied numerically with high accuracy for certain special cases with a free-particle representation. For example, the random XX model is equivalent via the Jordan-Wigner transformation to a problem of free fermions with random hoppings; the bipartite nature of the hopping leads to a ‘‘particle-hole’’ symmetry in the energy. Similarly the random transverse-field Ising model has been studied extensively and these numerical studies were strong support for the validity of the real-space renormalization group approach. In this section we will focus on numerical studies of entanglement entropy in random systems, then discuss in the following section some results on higher dimensions. (Note

that a numerical study of single-electron entanglement near the Anderson localization transition was already mentioned in Section 5.)

The theoretical calculation reviewed in Section 3 for the disorder-averaged critical entanglement entropy of the random XX model, which leads to a logarithmic divergence with effective central charge $\tilde{c} = c \ln 2$, was confirmed in a subsequent numerical study [75] on systems of up to 2000 sites. The difference between the entanglement for pure and random critical points is already clear for systems of a few hundred sites, but the larger systems are necessary to see that the divergence is indeed logarithmic. A key step in the calculation [76] is that the reduced density matrix is determined by the single-particle correlation matrix

$$\begin{pmatrix} \langle c_1^\dagger c_1 \rangle & \langle c_1^\dagger c_2 \rangle & \dots \\ \langle c_2^\dagger c_1 \rangle & \langle c_2^\dagger c_2 \rangle & \dots \\ \dots & & \dots \end{pmatrix} \quad (112)$$

which can be computed directly from the *single-particle* wavefunctions.

The conclusion that the counting of valence bonds using real-space renormalization group leads to the exact entanglement entropy for random singlet quantum critical points is at first glance surprising. For pure quantum critical points, it has been shown analytically and numerically [77] that “valence-bond” entropy and full entanglement entropy differ, although in those examples both have logarithmic divergences. The valence bond entanglement at random quantum critical points has been conjectured to appear also a universal prefactor appearing in correlation functions, with supporting numerical evidence [78]. (The ordinary correlation function receives nonuniversal contributions as well, but those authors propose a way to cancel the nonuniversal contributions by interfering sublattices.)

Recent work found an interesting relationship [79] between the entanglement entropy of random *quantum* critical points in one dimensions and the computational effort required in studying some classical spin glass models by the “simulated quantum annealing” approach. This result is somewhat similar in spirit to the “finite-entanglement scaling” [4, 5] at pure quantum critical points in one dimension, which is determined by the central charge [5] via the “entanglement spectrum” (the full set of density matrix eigenvalues [8]), which was recently determined for conformally invariant critical points [9]. The entanglement spectrum depends on a single parameter combining c and the correlation length, and determines the full set of Renyi entropies (which are essentially moments of the spectrum).

The entanglement spectrum at a random singlet quantum critical point can be conjectured to be rather simple and qualitatively different from the pure case, even though the entanglement entropy is similar. || For N bonds crossing the boundary, there are 2^N eigenvalues of value 2^{-N} , which leads to the disorder-averaged Renyi entropy

$$S_\alpha = \frac{1}{1-\alpha} \log_2 \left(\sum_i \lambda_i^\alpha \right) = \frac{1}{1-\alpha} \log_2 2^{N(1-\alpha)} = \log_2 N. \quad (113)$$

|| We thank P. Calabrese for conversations regarding this point.

(This just reflects the additivity of Renyi entropies for independent processes, where each singlet is an independent process.) Hence a numerical confirmation that the Renyi entropies are equal to the von Neumann entropy in the XX model would show that the random singlet model predicts not just the entanglement entropy but the universal part of the entanglement spectrum. The challenge may be to separate out this “universal part” from non-universal contributions, which is simple in the case of the entanglement entropy. It would then be interesting to confirm that the Renyi entropies are *not* trivially related to the von Neumann entropy in cases where the entanglement is not just a sum over independent singlet bonds.

7. Higher dimensions and other future directions

While entanglement entropy at higher-dimensional critical points is not understood as completely as in one dimension, there are several important results discussed elsewhere in this issue. In higher dimensions, many gapless systems show the same “area law” ($S \sim L^{d-1}$ for spatial dimensionality d) [3, 2] as for gapped phases. An exception is the entanglement for free fermions with a Fermi surface [14, 15], which has an additional logarithmic factor that can be related to the many gapless points on the Fermi surface. Beyond the area law contribution, interesting and sometimes universal subleading terms can appear at some critical points [80, 16, 81, 82]. One new aspect in higher dimensions is that the entanglement can have a nontrivial dependence on the geometry of the partition even for the case where one subsystem is a single contiguous region.

Understanding entanglement in some higher-dimensional critical points is possible through the strong-disorder renormalization group approach. Like all real-space renormalization approaches, dimensions greater than one are considerably more challenging, and some form of numerical analysis of the RG equations is typically necessary. Two studies to date of the two-dimensional random transverse-field Ising model reached different conclusions regarding entanglement at the model’s critical point. Lin, Igloi, and Rieger found a behavior of the entanglement consistent with an area law times a double logarithm, [83]

$$S(L) \approx L \log_2 \log_2 L + \dots, \quad (114)$$

and gave an argument for this result based on a picture of clusters in the strong-disorder renormalization group. (For a different model with a close connection to percolation, the bond-diluted transverse Ising model, these authors found an area law in all dimensions.) Yu, Saleur and Haas also studied the transverse-field Ising model RG equations numerically and found a different result: an area law plus a subleading single logarithm in the disorder-averaged entanglement entropy [84],

$$S(L) \approx \alpha L + \beta \log L + \dots, \quad (115)$$

with $\beta \approx -0.08 \pm 0.01$ and α nonuniversal. While this is superficially similar to the behavior at certain 2D quantum critical points [16], its physical origin is almost certainly different. The properties of the system were interpreted in terms of percolation

behavior, and properties of critical percolation clusters were shown analytically to give a logarithmic term of this form.

While a consensus is yet to emerge, these results do indicate that higher-dimensional critical entanglement entropies are an important remaining challenge: further aspects such as geometry dependence and the connection to other types of random critical points have yet to be studied. Other major challenges include a better understanding of the (classical and quantum) computational difficulty of random quantum systems and how this connects to entanglement, an understanding of dynamical and thermal properties of entanglement, and a more complete picture of how entanglement is manifested in experimental observations.

We hope that this review has conveyed some of the excitement regarding the new perspective that entanglement entropy offers on disordered quantum systems. The authors wish to thank many collaborators and colleagues for invaluable conversations over the past five years, and especially thank N. Bonesteel, P. Calabrese, E. Fradkin, L. Fidkowski, I. Klich, H.-H. Lin, S. Mukerjee, F. Pollmann, A. Silva, P. Titum, A. Turner, and K. Yang for their entanglement with the authors. The authors gratefully acknowledge financial support from the Packard Foundation, Research Corporation Cottrell award, and the Sloan Foundation, and NSF grants PHY-0456720 and PHY-0803371 (GR), and NSF DMR-0804413 (JEM).

- [1] Mark Srednicki. *Phys. Rev. Lett.*, 71:666, 1993.
- [2] M. B Hastings. *Journal of Statistical Mechanics: Theory and Experiment*, 08:24, 2007.
- [3] J Eisert, M Cramer, and M. B Plenio. *eprint arXiv*, 0808:3773, 2008.
- [4] L Tagliacozzo, Thiago. R de Oliveira, S Iblisdir, and J. I Latorre. *Physical Review B*, 78:24410, 2008.
- [5] Frank Pollmann, Subroto Mukerjee, Ari Turner, and Joel E Moore. *eprint arXiv*, 0812:2903, 2008.
- [6] D. L Moehring, P Maunz, S Olmschenk, K. C Younge, D. N Matsukevich, L.-M Duan, and C Monroe. *Nature*, 449:68, 2007.
- [7] Israel Klich, Gil Refael, and Alessandro Silva. *Physical Review A (Atomic, Molecular, and Optical Physics)*, 74(3):032306, 2006.
- [8] Hui Li and F. D. M Haldane. *Phys Rev Lett*, 101:10504, 2008.
- [9] Pasquale Calabrese and Alexandre Lefevre. *Physical Review A*, 78:32329, 2008.
- [10] C. Holzhey, F. Larsen, and F. Wilczek. *Nucl. Phys. B*, 424:44, 1994.
- [11] G. Vidal, J. I. Latorre, E. Rico, and A. Kitaev. *Phys. Rev. Lett.*, 90:227902, 2003.
- [12] P. Calabrese and J. Cardy. *J. Stat. Mech.*, 06:P06002, 2004.
- [13] Shinsei Ryu and Tadashi Takayanagi. *Phys. Rev. Lett.*, 96(18):181602, 2006.
- [14] D. Gioev and I. Klich. *Phys. Rev. Lett.*, 96:100503, 2006.
- [15] M. M. Wolf. *Phys. Rev. Lett.*, 96:010404, 2006.
- [16] E. Fradkin and J. E. Moore. *Phys. Rev. Lett.*, 97:050404, 2006.
- [17] A. B. Zamolodchikov. *JETP Lett.*, 43:731, 1986.
- [18] S. Sachdev. *Quantum phase transitions*. Cambridge University Press, London, 1999.
- [19] P. W. Anderson. *Phys. Rev.*, 109(5):1492–1505, 1958.
- [20] S. K. Ma, C. Dasgupta, and C. K. Hu. *Phys. Rev. Lett.*, 43:1434, 1979.
- [21] Curtis A. Doty and Daniel S. Fisher. *Phys. Rev. B*, 45(5):2167–2179, 1992.
- [22] R. N. Bhatt and P. A. Lee. *Phys. Rev. Lett.*, 48(5):344–347, 1982.
- [23] D. S. Fisher. *Phys. Rev. B*, 50:3799, 1994.
- [24] Ferenc Igloi and Cecile Monthus. *Phys. Rep.*, 412:277, 2005.
- [25] D. S. Fisher. *Phys. Rev. B*, 51:6411, 1995.

- [26] Daniel S. Fisher and A. P. Young. *Phys. Rev. B*, 58(14):9131–9141, 1998.
- [27] Gil Refael and Daniel S. Fisher. *Phys. Rev. B*, 70(6):064409, 2004.
- [28] N. E. Bonesteel and Kun Yang. *Phys. Rev. Lett.*, 99:140405, 2007.
- [29] Olexei Motrunich, Kedar Damle, and David A. Huse. *Physical Review B (Condensed Matter and Materials Physics)*, 65(6):064206, 2002.
- [30] Matthew S. Foster and Andreas W. W. Ludwig. *Physical Review B (Condensed Matter and Materials Physics)*, 73(15):155104, 2006.
- [31] C. Mudry, S. Ryu, and A. Furusaki. *Phys. Rev. B*, 67(6):064202, 2003.
- [32] K. Damle and D. A. Huse. *Phys. Rev. Lett.*, 89:277203, 2002.
- [33] C. Dasgupta and S. K. Ma. *Phys. Rev. B*, 22:1305, 1980.
- [34] G. Refael, S. Kehrein, and D. S. Fisher. *Phys. Rev. B*, 66:060402, 2002.
- [35] C. Monthus, O. Golinnelli, and Th. Jolicoeur. *Phys. Rev. B*, 58:805, 1998.
- [36] R. A. Hyman and K. Yang. *Phys. Rev. Lett.*, 78:1783, 1997.
- [37] I. Affleck, T. Kennedy, E. H. Lieb, and H. Tasaki. *Phys. Rev. Lett.*, 59:799, 1987.
- [38] N. Read and E. Rezayi. *Phys. Rev. B*, 59(12):8084–8092, 1999.
- [39] E. H. Rezayi and N. Read. *Physical Review B (Condensed Matter and Materials Physics)*, 79(7):075306, 2009.
- [40] A. Stern. *Ann. Phys. (N.Y.)*, 323:204–249, 2008.
- [41] A. Y. Kitaev. *Ann. Phys. (N.Y.)*, 303:2, 2003.
- [42] Eric Dennis, Alexei Kitaev, Andrew Landahl, and John Preskill. *Journal of Mathematical Physics*, 43(9):4452–4505, 2002.
- [43] Chetan Nayak, Steven H. Simon, Ady Stern, Michael Freedman, and Sankar Das Sarma. *Reviews of Modern Physics*, 80(3):1083, 2008.
- [44] L. Fidkowski, G. Refael, N. E. Bonesteel, and J. E. Moore. *Physical Review B (Condensed Matter and Materials Physics)*, 78(22):224204, 2008.
- [45] L. Fidkowski, H.-H. Lin, P. Titum, and G. Refael. *Physical Review B (Condensed Matter and Materials Physics)*, 79(15):155120, 2009.
- [46] X.G. Wen. *Quantum Field Theory of Many-Body Systems*. Oxford University Press, Oxford, 2004.
- [47] A. Feiguin, S. Trebst, A. W. W. Ludwig, M. Troyer, A. Kitaev, Z. Wang, and M. H. Freedman. *Phys. Rev. Lett.*, 98:160409, 2007.
- [48] S. Trebst, E. Ardonne, A. Feiguin, D. A. Huse, A. W. W. Ludwig, and M. Troyer. Collective states of interacting Fibonacci anyons. arXiv:0801.4602.
- [49] A. Furusaki, M. Sigrist, P. A. Lee, K. Tanaka, and N. Nagaosa. *Phys. Rev. Lett.*, 73(19):2622–2625, 1994.
- [50] A. Furusaki, M. Sigrist, E. Westerberg, P. A. Lee, K. B. Tanaka, and N. Nagaosa. *Phys. Rev. B*, 52(22):15930–15942, 1995.
- [51] Raoul Santachiara. *J.Stat. Mech.*, page L06002, 2006.
- [52] T. Senthil and Satya N. Majumdar. *Phys. Rev. Lett.*, 76(16):3001–3004, 1996.
- [53] G. Refael and J. E. Moore. *Phys. Rev. Lett.*, 93(26):260602, 2004.
- [54] G. Refael and J. E. Moore. *Physical Review B (Condensed Matter and Materials Physics)*, 76(2):024419, 2007.
- [55] José Abel Hoyos and E. Miranda. *Phys. Rev. B*, 70(18):180401, 2004.
- [56] J. S. Bell. *Physics*, 1:195, 1964.
- [57] Alain Aspect, Jean Dalibard, and Gérard Roger. *Phys. Rev. Lett.*, 49(25):1804–1807, 1982.
- [58] M. Lewenstein, B. Kraus, P. Horodecki, and J. I. Cirac. *Phys. Rev. A*, 63(4):044304, 2001.
- [59] Barbara M. Terhal. *Physics Letters A*, 271(5-6):319 – 326, 2000.
- [60] Radim Filip. *Phys. Rev. A*, 65(6):062320, 2002.
- [61] Israel Klich and Leonid Levitov. *ADVANCES IN THEORETICAL PHYSICS: Landau Memorial Conference*, 1134(1):36–45, 2009.
- [62] Israel Klich and Leonid Levitov. *Physical Review Letters*, 102(10):100502, 2009.

- [63] R. Balian. *Eur. J. Phys.*, 10:208–213, 1989.
- [64] John M. Martinis, S. Nam, J. Aumentado, and C. Urbina. *Phys. Rev. Lett.*, 89(11):117901, 2002.
- [65] Lara Faoro and Lev B. Ioffe. *Physical Review Letters*, 100(22):227005, 2008.
- [66] Magdalena Constantin, Clare C. Yu, and John M. Martinis. *Physical Review B (Condensed Matter and Materials Physics)*, 79(9):094520, 2009.
- [67] Lara Faoro, Joakim Bergli, Boris L. Altshuler, and Y. M. Galperin. *Phys. Rev. Lett.*, 95(4):046805, 2005.
- [68] Rogerio de Sousa. *Physical Review B*, 76:245306, 2007.
- [69] P. W. Anderson. *Phys. Rev.*, 109:1492–1505, 1958.
- [70] A MacKinnon and B Kramer. *Phys Rev Lett*, 47:1546, 1981.
- [71] F Evers and A Mirlin. *Rev. Mod. Phys.*, 2008.
- [72] K Slevin, P Markos, and T Ohtsuki. *Phys Rev Lett*, 2001.
- [73] Angela Kopp, Xun Jia, and Sudip Chakravarty. *Annals of Physics*, 322:1466, 2007.
- [74] Xun Jia, Arvind R Subramaniam, Ilya A Gruzberg, and Sudip Chakravarty. *Physical Review B*, 77:14208, 2008.
- [75] Nicolas Laflorencie. *Physical Review B*, 72:140408, 2005.
- [76] Ming-Chiang Chung and Ingo Peschel. *Physical Review B (Condensed Matter and Materials Physics)*, 64:64412, 2001.
- [77] J Jacobsen and H Saleur. *Phys Rev Lett*, 2008.
- [78] José A Hoyos, André P Vieira, N Laflorencie, and E Miranda. *Physical Review B*, 76:174425, 2007.
- [79] J Rodríguez-Laguna. *Journal of Statistical Mechanics: Theory and Experiment*, 05:8, 2007.
- [80] Shinsei Ryu and Tadashi Takayanagi. Holographic Derivation of Entanglement Entropy from AdS/CFT. unpublished; arXiv:hep-th/0603001, 2006.
- [81] Benjamin Hsu, Michael Mulligan, Eduardo Fradkin, and Eun-Ah Kim. *Physical Review B*, 79:115421, 2009.
- [82] Max A. Metlitski, Carlos A. Fuertes, and Subir Sachdev. Entanglement Entropy in the O(N) model, 2009.
- [83] Yu-Cheng Lin, Ferenc Iglói, and Heiko Rieger. *Phys Rev Lett*, 99:147202, 2007.
- [84] Rong Yu, Hubert Saleur, and Stephan Haas. *Physical Review B*, 77:140402, 2008.